nature photonics

SUPPLEMENTARY INFORMATION
https://doi.org/10.1038/s41566-018-0234-0

In the format provided by the authors and unedited.

Photography optics in the time dimension

Barmak Heshmat[1]*, Matthew Tancik[2], Guy Satat[1] and Ramesh Raskar[1]

[1]Media Lab, Massachusetts Institute of Technology, Cambridge, MA, USA. [2]Computer Science and Electrical Engineering, Cambridge, MA, USA.
*e-mail: barmak@mit.edu

Supplementary information

Photography optics in the time dimension

<u>Temporal image formation model</u>

Consider a thin spherical lens with focal length *f*, curvature radius *R'*, thickness d_l, refractive index *n*, and radius *r*, such that $r \leq \sqrt{2R'd_l - {d_l}^2}$, $R' > 0.5d_l$, $f = R'/(n-1)$. For such thin lens imaging system with the distance between the lens and sensor being time-folded, one can find the temporal image formation model as follows; consider a point source in the scene parameterized by $P1 = (x_{P1}, \nu_{P1}, t_{P1})$ where x is position, ν is angle and t is time (Supplementary Fig. 1 a). After propagation of a distance u to the lens plane, the light rays will be at $P2 = (x_{P2}, \nu_{P2}, t_{P2}) = (x_{P1} + \nu_{P1}u,\ \nu_{P2},\ t_{P1} + \frac{u}{c}\sqrt{1 + {\nu_{P1}}^2})$ by passing through the lens the rays will pass through *P3* found as:

$$P3 = (x_{P3}, \nu_{P3}, t_{P3}) = \left(x_{P2}, \nu_{P2} - \frac{x_{P2}}{f}, t_{P2} + \frac{d_l - R' + \sqrt{R'^2 - {x_{P2}}^2}}{cn}\right). \qquad (1)$$

After passing through the cavity with length *d* the exiting ray at the *m*th round-trip can be found by Supplementary Equation (2).

$$P4 = (x_{P4}, \nu_{P4}, t_{P4}) = \left(x_{P3} + \nu_{P3}(2m+1)d, \nu_{P3}, t_{P3} + \frac{(2m+1)d}{c}\sqrt{1 + {\nu_{P3}}^2}\right) \qquad (2)$$

Finally, combining the equations for $P1 - P4$ the output of the cavity for a point source at $P1 = (x_{P1} = x, \nu_{P1} = \nu,\ t_{P1} = t)$ is:

$$\left(x + \nu u + \left(\nu - \frac{x+\nu u}{f}\right)(2m+1)d, \nu - \frac{x+\nu u}{f}, t + \frac{u}{c}\sqrt{1+\nu^2} + \frac{d - R' + \sqrt{R'^2 - (x+\nu u)^2}}{cn} + \frac{(2m+1)d}{c}\sqrt{1 + \left(\nu - \frac{x+\nu u}{f}\right)^2}\right) \quad (3)$$

Using this approach and considering a Gaussian temporal profile for the pulse, the streak image can be estimated as in Supplementary Fig. 1 b. This is slightly different from what's measured in Fig. 2 a and b due to initial temporal profile of the illuminated scene. Supplementary Figure 1 c shows how the decay profile can differ with the choice of reflectivity. Recording higher number of round-trips is a trade-off between dynamic range, noise level, and choice of reflectivity and loss (Supplementary Fig. 1 d). Higher reflective facets push larger number of round-trips into the dynamic range of the sensor but require larger gain. With our streak sensor we could measure ~30 round-trips at most with two OD 3 ND filters (R = 0.68) as facets of the cavity. Higher round-trips are more alignment sensitive as angular deviation from optical axis of the cavity aggregates with each round-trip.

Ultrafast light-field sampling

The design with the cavity behind the lens can also act as a means to measure the focal stack at the time resolution of the streak camera and cavity size. This is evident by considering the modified lens equation for a time-folded system as for each value of *m*, a different *o*(*t*) will be in focus.

$$\frac{\boldsymbol{1}}{\boldsymbol{f}} = \frac{\boldsymbol{1}}{\mathrm{o(t)}} + \frac{\boldsymbol{1}}{\boldsymbol{c}((\boldsymbol{2m}+\boldsymbol{1})\boldsymbol{d}/\boldsymbol{c}+d'/\boldsymbol{c})} \rightarrow o\,(t_m) = 1/\left(\frac{1}{f} - \frac{1}{(2m+1)d+d'}\right) \quad (4)$$

This indicates that larger, higher round-trips focus on closer objects and the speed of transition from one slice of the focal stack to the next equals the round-trip time of the cavity. Such a high speed of transition is not obtainable with any mechanical scanning method and can be taken advantage of in volumetric scenes with ultrafast dynamics (e.g., 3D light-matter interactions, ultrafast tomography, and light propagation measurements). These measurements can also provide a means to real-time focal stack for scenes with slower dynamics (e.g., study of low-speed phase objects, real-time diffuse optical tomography, etc.). On the other hand, if the scene is sparse in the temporal domain, then each of the round-trips can be considered as a sample of the evolving wavefront in the fractional Fourier domain. This can help to reconstruct the light-field inside the lens system to study the aberration or wavefront distortions as shown in the Supplementary Fig. 2 (a1-a5). Here a laser beam is expanded with a microscope objective and a convex lens, and then fed to a slightly misaligned lens. The trace intensity patterns in time can provide 3D information about the profile of the light field and indicate alignment status.

Transfer matrix for lens inside the cavity

An explicit m^{th} round-trip transfer matrix M_m for the case of lens inside the cavity (as in the case of multi-zoom camera) is estimated as:

$$M_m = M_{0.5d} P C^{(m-1)} P^{-1} M_{0.5d}\ ,$$

$$P = \begin{bmatrix} \frac{1}{2}\left(\sqrt{d(d-4f)} - d\right) & -\frac{1}{2}\left(\sqrt{d(d-4f)} + d\right) \\ 1 & 1 \end{bmatrix}$$

$$C = \frac{1}{2f}\begin{bmatrix} -\left(d - 2f + \sqrt{d(d-4f)}\right) & 0 \\ 0 & \left(2f - d + \sqrt{d(d-4f)}\right) \end{bmatrix} \qquad (5)$$

$$P^{-1} = \frac{1}{\sqrt{d-4f}}\begin{bmatrix} \frac{1}{\sqrt{d}} & \frac{\sqrt{d} + \sqrt{d-4f}}{2} \\ \frac{-1}{\sqrt{d}} & \frac{\sqrt{d}\sqrt{d-4f} - d}{2\sqrt{d}} \end{bmatrix}$$

As noted, the diagonal matrix C is the only matrix that is multiplied by itself as the number of round-trips increases. The elements of this matrix can become imaginary if $d<4f$ but this does not invalidate this expression as C and P are only auxiliary matrices to assist calculating the final transmission matrix in a compact explicit form for a higher number of round-trips. C and P do not physically represent any one element in the system. The full-field expression is also obtainable for the resonant case as indicated in reference 20 of the manuscript.

Lens position inside the cavity

Similar to lens focal length and cavity length, the lens position in the cavity can also have notable effect on the stability and degeneracy of the optical cavity. This is even more pronounced when looking at the cavity at ultrafast speeds as the output field is not time averaged, similar to a resonant cavity. Supplementary Figure 3 shows the dynamics of the effective focal length of a 15 cm cavity with the lens position varying inside it. The dynamics of the effective focal length with round-trip number will look similar to one of the three graphs as in Supplementary Fig. 3 depending on the relative values of d and f.

Scalable uni-axial design for time-folded multi-spectral imaging

In our demonstration, we showed multi-spectral ultrafast imaging by dividing the aperture and time-folding each side differently (Fig. 4 b). We chose that design over the one in Fig. 4 a, since it does not require specific spectral profiles of the filters and thus can be easily realized with commercial elements placed further away, side by side, in front of the lens. An improved design would use customized notch reflective filters in the arrangement shown in Supplementary Fig. 4 to benefit the entire aperture of the camera for the entire spectrum. The uniaxial design is easily scalable as in theory any desired number of filters can be stacked in the front cavity as long as the time-resolution of the camera allows. Supplementary Figure 4 c shows the temporal profile after the first pass through the time-folded multispectral imaging optics used to capture the fluorescent scene in Supplementary Video 4. As seen in the video, the UV pulses excite the fluorescent patch from the left side. The time-folded system captures the rise and fall time of the fluorescent material along with location and direction of scattering. The data shows that because of different round-trips for UV and visible light, one can capture the rise time, peak intensity, and lifetime of the fluorescent area along with its UV reflection in the same acquisition for each pixel. The UV peak provides information about excitation spatial and temporal profile while the fluorescent signal provides information about the fluorophore. Finally, other than time gating; computational methods can be used to extract less sparse signals with better efficiency.

Other potential limitations

The thickness of optics and the surface reflection of optics can be considered as an interference factor. This is noted in the streak images in Fig. 2 b, 3 c and 4 c. The same interference also indicates that one may be able to simply implement the time-folding by applying reflective coatings to the imaging lens or using a single glass slab with a semi-reflective coating on both sides. The aberration and dispersive behavior of the elements inside the cavity will build up for a larger number of round-trips. This undesired effect can be addressed with aberration correcting elements after the cavity.

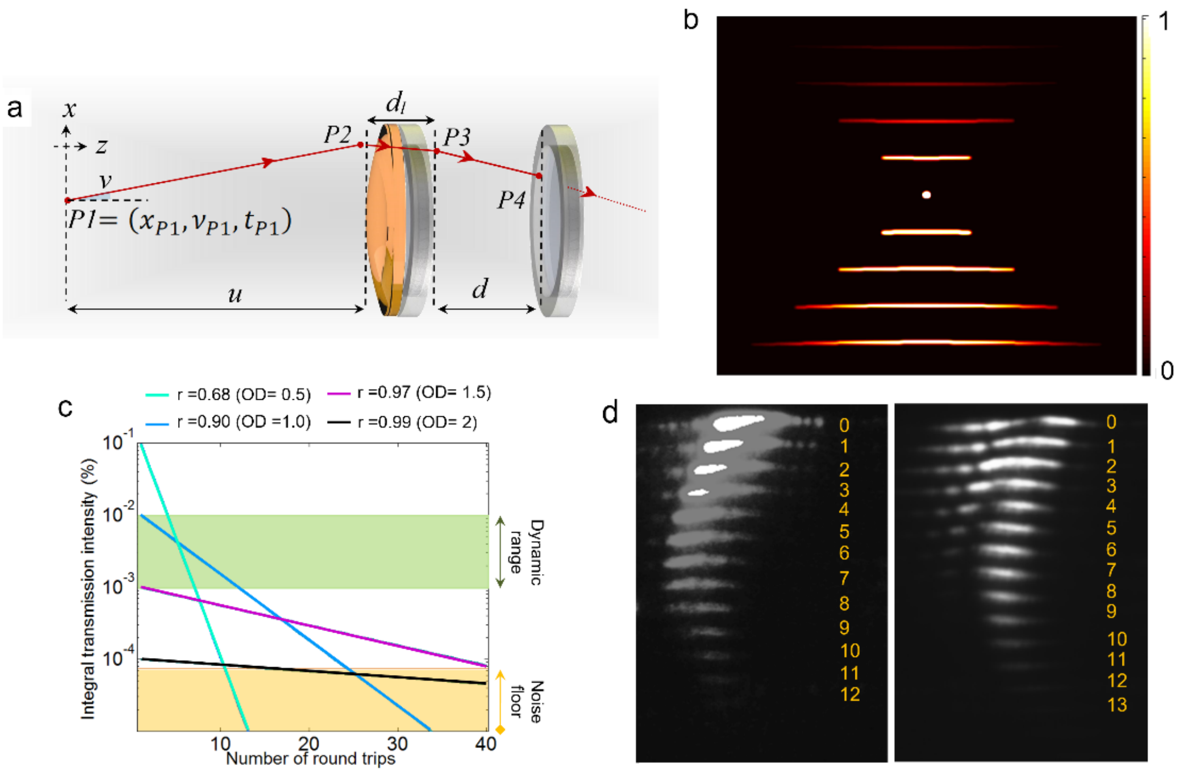

Supplementary Figure 1 | Streak formation model for a point source. a, Light path for the first pass through the system goes through the P1, P2, P3, P4 points. Here P4 is shown for the first pass. **b,** Simulated streak images using the proposed forward model. The spherical wavefront from a perfect point source with a Gaussian temporal profile is focused into a point. The lens is considered to have slight Gaussian vignetting. **c**, Intensity variation based on choice of OD (or reflectivity) for loss-less cavity facets, higher OD will enable higher number of round-trips to be measurable with the camera but the measurements will be closer to the noise floor and will require higher gain. **d,** Streak images of the light exiting the time-folded compressed lens (cavity made with two OD 2 facets, T =0.01, R = 0.67, α' = 0.32). Capturing images at higher orders can be limited by dynamic range (left) or noise floor (right) depending on loss per round trip.

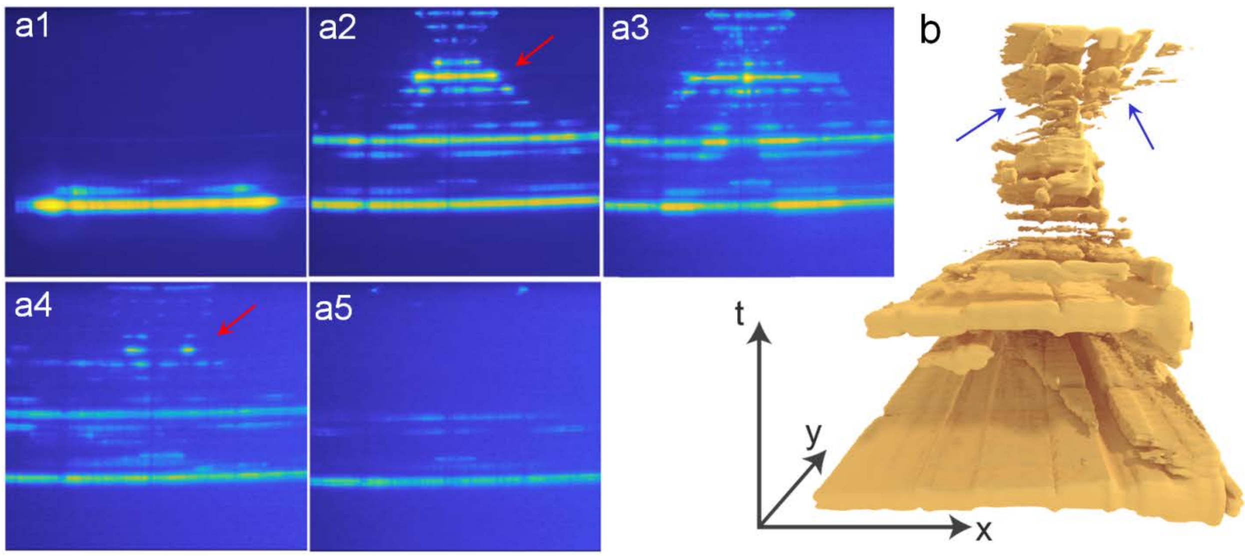

Supplementary Figure 2 | Probing wavefront distortion. a1-a5, *x-t* streaks at different *y* of the data cube and reconstructed 3D light field. The misalignment is evident by comparing the difference in a2 and a4. The trace reflections are formed by the glass thickness of the cavity. The helix shapes observed at the a3 cross section indicates Fresnel rings of the collimated laser light created by misalignments in the beam expander elements (see Supplementary Video 2). **b**, 3D light-field profile inside the lens system sampled at different depth (or time) by a FP cavity between the lens and ultrafast sensor. The blue arrows indicate the a2 and a4 cross sections and the asymmetry that is evident in the 3D representation.

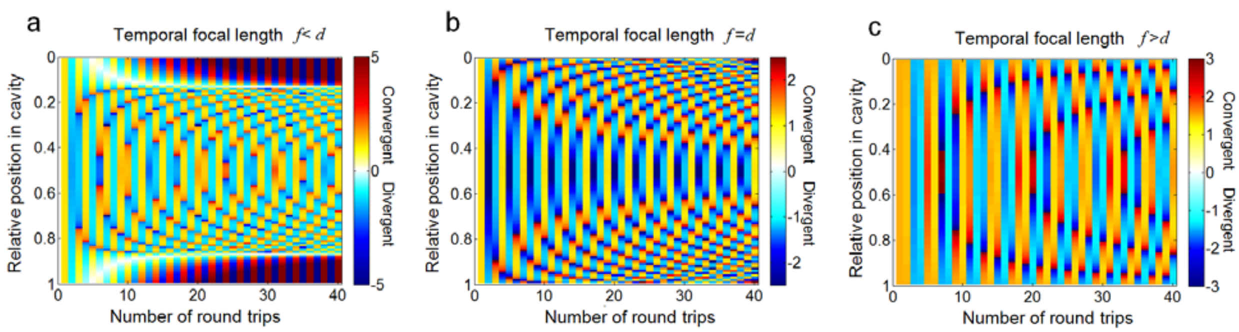

Supplementary Figure 3 | Effective focal length of a time-folded imaging system with lens position varying inside the cavity and number of round-trips. The effective focal length in log scale when: **a**, focal length is smaller than cavity length (e.g., here f = 13 cm and d = 15 cm). **b**, focal length is equal to cavity length (e.g., here f = d = 15 cm). **c**, focal length is larger than cavity length (e.g., here f = 30 cm and d = 15 cm). The cool color map refers to divergence of wavefront and hot color map shows the convergent focal length. The white regions shows collimating behavior where the input beam is collimated. The vertical axis is the relative lens position normalized from 0 to 1; therefore, the lens is in the middle of the cavity at 0.5. This explains the vertical symmetry of the graphs around 0.5 value.

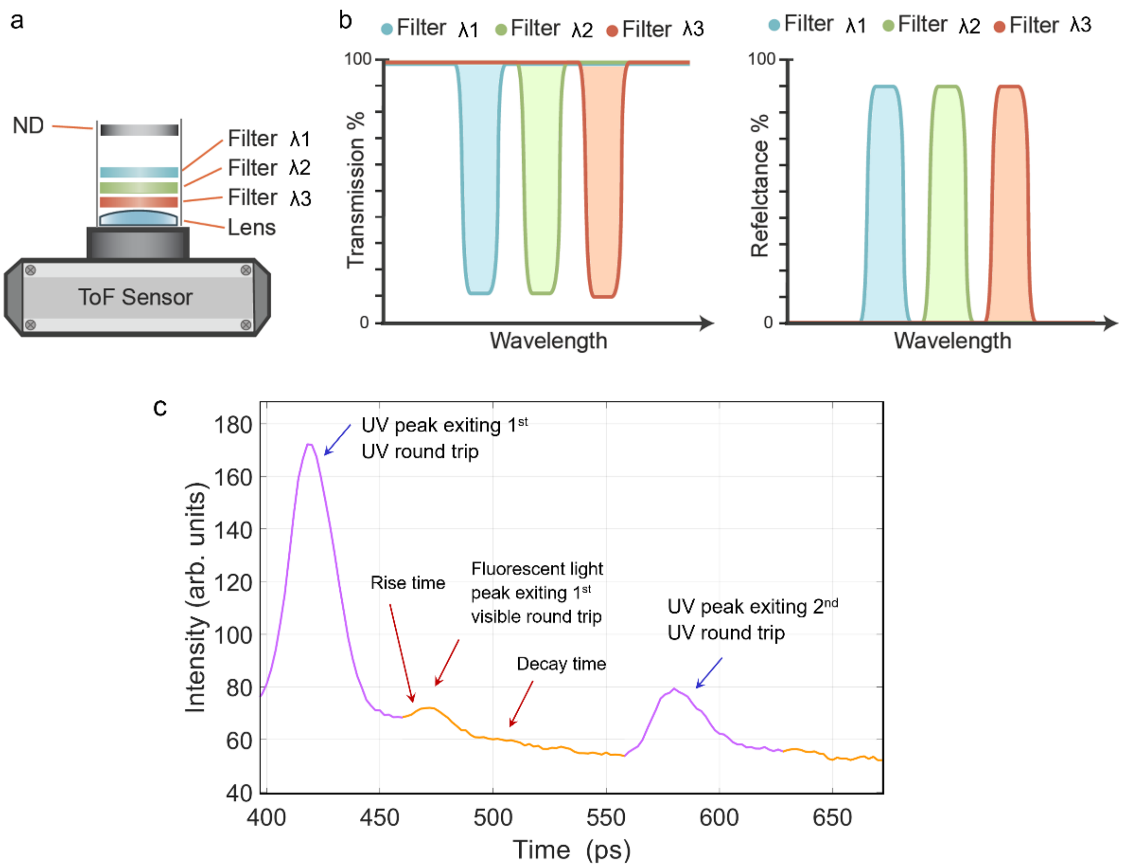

Supplementary Figure 4 | Uniaxial time-folded design for multi-spectral imaging optics. a, Design schematics. All filters benefit the entire FoV and aperture of the imaging optics. **b,** Ideal required transmittance and reflectance spectral profile of each notch reflector (0.9 reflectivity). The front ND is considered to be broad band; partially reflecting all the frequencies uniformly. **c,** Temporal dynamics captured for an arbitrary pixel in Supplementary Video 4 on fluorescent scene.

Supplementary Video 1 | Imaging with time-folded compressed lens tube. Each frame of the video refers to a 2 ps time step. At 5th round-trip the camera captures the scene in focus along with its temporal signature. At the end of the video what a normal (slow) camera would capture is shown for comparison.

Supplementary Video 2 | Time-folding enables capturing the evolution of the wavefront in the optical system. Each frame is a streak *x*-*t* image taken at a different *y*. The cavity samples various stages of the field evolving inside the optics. Same technique can be considered equivalent to capturing focal stack of the light passing through a 3D scene volume.

Supplementary Video 3 | Turning streak camera to multispectral IR imaging camera using time-folding. The letters A and B are illuminated with two different wavelengths. Based on the periodicity of exiting wavefront from a frequency-dependent time-folded optics one can extract the frequency contributions at each pixel in the same acquisition.

Supplementary Video 4 | Turning streak camera to multispectral fluorescence lifetime imaging (FLIM) camera using time-folding. The fluorophores patch is illuminated with UV pulses. Based on the periodicity of exiting wavefront from a frequency-dependent time-folded optics one can extract the frequency contributions along with spatial and temporal information at each pixel in the same acquisition.